Single-molecule Aflatoxin B1 Sensing via Pyrrole-based Molecular Quantum Dot

Single-molecule Aflatoxin B1 Sensing via Pyrrole-based Molecular Quantum Dot

Fabrizio Mo*†§, *Graduate Student Member, IEEE*, Chiara Elfi Spano*†, Yuri Ardesi†, *Graduate Student Member, IEEE*, Massimo Ruo Roch†, Gianluca Piccinini† and Mariagrazia Graziano‡

***Abstract*— We investigate through *ab-initio* simulations the gold-8PyrroleDiThiol-gold (Au-8PyDT) molecular quantum dot as an amperometric single-molecule sensor for the aflatoxin B1 (AFB1) detection. We study the adsorption of AFB1 onto the Au-8PyDT and we analyze the transport characteristics for the most probable adsorption configuration. We find that a significant current modulation occurs, with around 80% of current decrease in presence of AFB1. Interestingly, the investigated sensor exhibits a voltage-dependent response, that we motivate through a transmission properties analysis. Our results, considering the synthesis simplicity of PolyPyrroles and their non-toxicity, motivate future research efforts in this direction.**

I. Introduction

Aflatoxins are dangerous oncogenic and immunosuppressive mycotoxins, mainly produced by *Aspergillus flavus* and *Aspergillus parasiticus* fungi. Among them, aflatoxin B1 (AFB1) is most frequently present in contaminated samples, and it is in the Group I of carcinogenic to humans [1], [2].

Conventional aflatoxin detection techniques require bulky high cost instrumentation, long test times, skilled researches and also the usage of labels. Research efforts are toward developing novel detection techniques with high sensitivity and fast response, permitting a high degree of automatization in the measurement process. To this purpose, new biosensors, exploiting nanotechnology and nanomaterials, were developed with unique advantages, even if drawbacks are still present: the high fabrication cost, the toxicity of the employed nano-elements, and the complex electrode modification and functionalization requirement [3], [4]. Furthermore, the sensitivity is limited by the use of large bio-molecules as detecting elements (like conventional antibodies). A promising direction to overcome the latter limit is the use of smaller detecting elements, like nano-body molecules [4].

In this scenario, single-molecule detection is becoming a reality, reaching the ultimate limit of sensitivity, i.e., the detection of single-entities of chemical compounds, with the promising advantages of being intrinsically calibration-free and extremely sensitive [5], [6]. Also, the recent advancements of supra- and single-molecule electronics are filling the gap between theoretical investigations and prototyping, with the development of a variety of electronic devices based on molecular and functionalized structures [7]–[9].

*The two authors contributed equally to this work

†*Department of Electronics and Telecommunications, Politecnico di Torino, Torino, Italy*

‡*Department of Applied Science and Technology, Politecnico di Torino, Torino, Italy*

§ corresponding author e-mail: *fabrizio.mo@polito.it*

In this work, we investigate the gold-8-Pyrrole-DiThiol-gold molecular dot (Au-8PyDT) as an amperometric Single-Molecule Sensor (SMS) for AFB1 detection. Thanks to its intrinsic structure, the device under study is promising for real-time, and on-site AFB1 detection, with potential low production cost [10] and high sensitivity, since it lowers the limit of detection to a single-molecule. The proposed Au-8PyDT SMS goes toward a highly miniaturized sensing element to boost the sensitivity, paving the way toward monitoring AFB1 in food stocks and on field. Furthermore, the poly-pyrrole is proved to be biocompatible and non-toxic, overcoming the drawback of toxicity of commonly used nanomaterials [11], [12].

II. Methodology and Computational Details

We investigate a pyrrole-based molecular dot, since polypyrroles are known to present conductive properties similar to semiconducting or insulating materials, depending on the synthesis process and doping [13]. Furthermore, they are proved to change their conductance in presence of both inorganic (NO, CO_2, CO, NH_3, H_2S) and some organic (acetone, methanol, ethanol) compounds [13]. Fig. 1(a) shows the sensor under study. It is a single-molecule quantum dot constituted by a single 8-pyrrole-dithiol (8PyDT) molecule anchored through the Au-S bonds to two gold FCC (111) electrodes (Au-8PyDT), resembling metal-molecule-metal break-junctions [14]. Fig. 1(b) shows the AFB1 molecule.

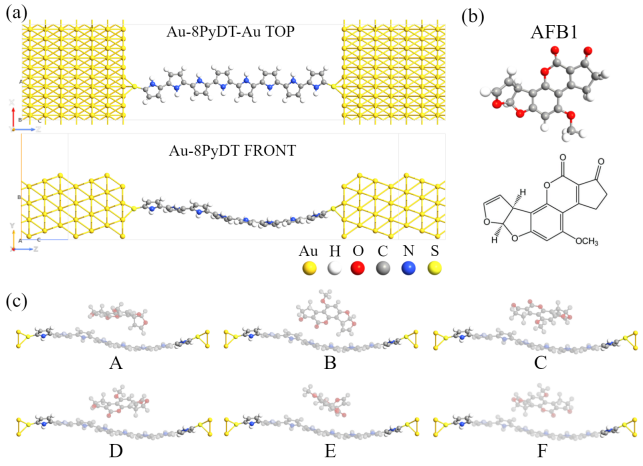

Fig. 1. (a) Top and front view of the Au-8PyDT sensor; (b) AFB1 molecule $(C_4H_4N)_8$2SH and its structural formula; (c) The studied geometries with different relative orientations of AFB1 w.r.t. the Au-8PyDT after the geometry optimization. Bright atoms are fixed during the relaxation, while for the others no constraint is enforced.

We perform the geometry optimizations of the isolated 8PyDT and AFB1 molecules in the quantum chemistry package ORCA [15] within the framework of the unrestricted Density Functional Theory (DFT) with the Generalized Gradient Approximation (GGA); exchange-correlation functional: Becke, 3-parameter, Lee–Yang–Parr (B3LYP). The van der Waals (vdW) correction DFT-D3 is enabled and the used basis set is the polarized valence triple-ζ (def2-TZVP).

To study the adsorption of the AFB1 onto the Au-8PyDT sensor, the geometry optimizations of six different relative orientations of AFB1 w.r.t. the Au-8PyDT, covering all possible significant adsorption configurations, are carried out in QuantumATK [16] - Fig. 1(c). To this purpose, we use DFT within the GGA, Perdew–Burke–Ernzerhof (PBE) exchange-correlation functional, and polarized double-ζ (DZP) basis set for all elements except for gold, for which we use polarized single-ζ (SZP) basis set. To reduce the computational time we account for the whole gold electrodes by enforcing fixed atom boundary conditions in the two lateral regions of a reduced Au-8PyDT geometry - Fig. 1(c). The AFB1 and central backbone of the 8-PyDT are left to freely relax without constraints. The geometries are relaxed using the LBFGS method for the energy minimization until the force on each atom becomes smaller than $0.05\,\mathrm{eV/\AA}$. The vdW Grimme D3 and the counterpoise (CP) correction for Basis Set Superposition Error (BSSE) are enabled. We evaluate the adsorption energy E_{ads} as:

$$E_{ads} = E_{AFB1/SMS} - [E_{AFB1} + E_{SMS}] \qquad (1)$$

where $E_{AFB1/SMS}$ is the total energy for the AFB1 adsorbed onto the Au-8PyDT SMS, E_{AFB1} and E_{SMS} are the total energy of the isolated AFB1 and Au-8PyDT SMS, respectively.

Electronic structure properties of the Au-8PyDT SMS in presence and absence of the adsorbed AFB1 molecule are studied in QuantumATK employing DFT with GGA, PBE, vdW D3 correction, SZP for Au and DZP for other elements. The system electrostatics is modeled by solving the Poisson equation using conjugate gradient method and with periodic boundary conditions in the transverse horizontal direction to account for the electrode periodicity. Dirichlet boundary conditions are instead enforced in the transport direction and along the transverse vertical direction to avoid artifacts due to presence of AFB1 molecule. The transport calculations are performed within the well-established Non-Equilibrium Green's Function (NEGF) formalism. Thanks to the covalent Au-S bonds between the 8-PyDT molecule and electrodes, high electron delocalization through the system is ensured and molecule-electrode strong coupling regime holds with the broadening of the molecular energy levels. Therefore, the main transport mechanism is coherent tunneling and the Drain-to-Source current I_{DS} is computed through the well-known Landauer formula [17]:

$$I_{DS} = \frac{2q}{h} \int_{-\infty}^{+\infty} T(E, V_{DS}) \left[f_S(E) - f_D(E) \right] dE \qquad (2)$$

where q is the electron charge, h is the Planck constant, E is the electron energy, V_{DS} the applied voltage, f_S and f_D are source and drain Fermi-Dirac distributions, respectively. $T(E, V_{DS})$ is the transmission function representing the electron transmission probability of the device. Notice that $T(E, V_{DS})$ is function of both the electron energy E and the applied voltage V_{DS}.

We evaluate the sensor response to AFB1 through the I_{DS} variation and percentage variation, defined respectively as:

$$\begin{aligned} \Delta I_{DS} &= I_{DS,AFB1} - I_{DS,0} \\ \Delta I_{DS\%} &= \left[\left(I_{DS,AFB1} - I_{DS,0} \right) / I_{DS,0} \right] \cdot 100 \end{aligned} \qquad (3)$$

where $I_{DS,0}$ is the current of the Au-8PyDT SMS, and $I_{DS,AFB1}$ is the current of the Au-8PyDT SMS in presence of AFB1. Notice that a positive ΔI_{DS} indicates an increase of current, whereas a negative ΔI_{DS} indicates a decrease.

We postpone to future works the selectivity study in presence of other mycotoxins or additional chemical compounds.

III. Results and discussion

Table I reports the calculated adsorption energies E_{ads}, as defined in equation (1), for all the considered adsorption configurations (Fig. 1(c)). The obtained E_{ads} values are greater in magnitude than the typical vdW weak physisorption energies (usually in the range 1÷30 kJ/mol), but below the typical chemisorption ones (100÷1000 kJ/mol) [18]. The obtained E_{ads} values match the binding energy range of hydrogen bonds (1÷170 kJ/mol) [19]. Therefore, we conclude that in all cases the AFB1 is strongly physisorbed onto the Au-8PyDT with the creation of hydrogen bonds, as already experimentally verified between AFB1 and DNA/aptamers with binding energies of the same order of the obtained E_{ads} [20], [21]. We believe the hydrogen bonds to originate between the AFB1 carbonyl or methoxy groups and the NH secondary amines of the 8-PyDT, with the latter acting as proton donor. We postpone the detailed investigation on the adsorption bond nature to future works. Among the possible adsorption configurations, the most stable and probable is geometry F (lowest E_{ads}). Consequently, in the following, we analyze the transport only in the case of geometry F.

TABLE I
CALCULATED E_{ads} VALUES.

geometry	E_{ads} (kJ/mol)	geometry	E_{ads} (kJ/mol)
A	-58.96	D	-69.09
B	-53.56	E	-55.74
C	-59.81	F	-75.52

Fig. 2(a) reports the $I_{DS}(V_{DS})$ characteristics in presence and absence of AFB1. The presence of AFB1 decreases the current, especially in the range $0\,\mathrm{V} \div 0.5\,\mathrm{V}$ and in the peak around $1\,\mathrm{V}$. Whereas, at $0.7\,\mathrm{V}$ and above $1.3\,\mathrm{V}$ the $I_{DS,0}$ and $I_{DS,AFB1}$ are quite similar. Fig. 2(b) reports the absolute and relative current modulations as defined in equation (3). Both ΔI_{DS} and $\Delta I_{DS\%}$ are negative ($I_{DS,AFB1}$ is always lower than $I_{DS,0}$) with minima for two different V_{DS} values. In particular, the maximum current modulation

occurs at 1 V, in which $I_{DS,AFB1}$ is 0.626 µA lower than $I_{DS,0}$ ($I_{DS,AFB1}$=1.49 µA versus $I_{DS,0}$=2.116 µA). Nevertheless, due to the greater current values achieved for this voltage, the percentage modulation of current results to be only 29.6%. The greatest percentage modulation of current occurs instead at around 0.4 V, where $\Delta I_{DS\%}$ reaches the 83.87% of current reduction in presence of AFB1. The corresponding ΔI_{DS} is -0.26 µA ($I_{DS,AFB1}$=0.05 µA versus $I_{DS,0}$=0.31 µA). Therefore, a good operating voltage for the AFB1 detection is 0.4 V. Indeed, at $V_{DS} = 0.4$ V there is an evident reduction of current in presence of AFB1, with an $I_{DS,AFB1}$ about one fifth of the $I_{DS,0}$. Current variations of this order are measurable through integrated CMOS front-end electronics [22].

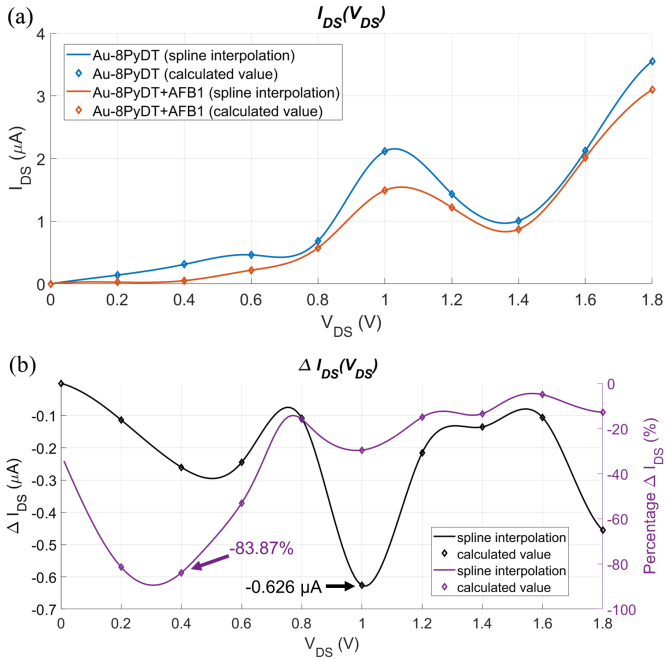

Fig. 2. (a) Current-voltage characteristics of the Au-8PyDT with and without AFB1. The spacing of the simulated values is 0.2 V. They are interpolated with a cubic spline function; (b) ΔI_{DS} (black) and $\Delta I_{DS\%}$ (purple).

Interestingly, the sensor response is voltage-dependent. Indeed, the AFB1 causes a current reduction that varies with V_{DS}, from few nA (-4.98%) to hundreds nA (-83.87%). The origin of the sensor voltage-dependent response is explained by considering the V_{DS} effect in equation (2). A positive V_{DS} lowers the drain Fermi level (E_{FD}) w.r.t. the source one (E_{FS}) of an amount $-qV_{DS}$ ($E_{FD} = E_{FS} - qV_{DS}$). We call the Fermi level shift Bias Window (BW): $BW = qV_{DS}$, as in Fig. 3(a). The V_{DS} affects equation (2) through the Fermi function difference:

$$f_S(E) - f_D(E) = \frac{1}{e^{\frac{E-E_{FS}}{kt}} + 1} - \frac{1}{e^{\frac{E-E_{FS}+qV_{DS}}{kt}} + 1} \quad (4)$$

where k is the Boltzmann constant and t the temperature. For increasing V_{DS} values, an increasing number of occupied electron states at the source finds empty states at the drain, in which they can tunnel. As a result, a current originates if f_S and f_D are unbalanced with occupied states at source and empty states at drain, and $T(E, V_{DS})$ is large enough to ensure a significant Source-to-Drain transmission probability. Therefore, the effect of the Fermi function difference in equation (2) is to weight the transmission function $T(E, V_{DS})$, as depicted in Fig. 3(a). For energies E inside or close the BW, the Fermi function difference is close to unity ($f_S(E) - f_D(E) \approx 1$), while for energies E distant from the BW it is close to zero ($f_S(E) - f_D(E) \approx 0$).

For a SMS, three main cases may occur: (i) The presence of the target molecule modifies $T(E, V_{DS})$ around the BW. In this case the current variations ΔI_{DS} and $\Delta I_{DS\%}$ will be large - Fig. 3(b). (ii) The presence of the target modifies $T(E, V_{DS})$ at energies distant from the BW. In this case ΔI_{DS} and $\Delta I_{DS\%}$ will be small - Fig. 3(c). (iii) The presence of the target modifies $T(E, V_{DS})$ around the BW, but in a way that the $T(E, V_{DS})$ variations compensate. In this case, since the current is related to integral in energy of $T(E, V_{DS})$, the obtained ΔI_{DS} and $\Delta I_{DS\%}$ will be still small - Fig. 3(d). Therefore, depending on the applied voltage V_{DS}, significant variations of $T(E, V_{DS})$ can be included in the BW, resulting in significant ΔI_{DS} and $\Delta I_{DS\%}$.

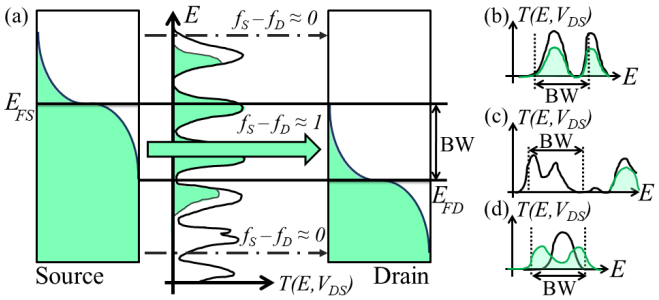

Fig. 3. (a) BW and Fermi function weighting effect on $T(E, V_{DS})$; (b), (c), (d) Examples of different target effects: green and black curves are referred to the cases in which the target is present and absent, respectively.

To explain the origin of current reduction in presence of AFB1 we investigate the $T(E, V_{DS})$ in the two bias points of interest, i.e., 0.4 V and 1 V - Fig. 4(a) and (b). The vertical dashed lines highlight the BW. At $V_{DS} = 0.4$ V (Fig. 4(a)), the dashed line centered in 0.2 eV corresponds to the source Fermi level position while the one in -0.2 eV to the drain one. Notice that the Fermi-Dirac distribution "tails" broaden the energy integration range slightly outside this range. The AFB1 affects the transmission function in two ways: (i) the transmission peaks are shifted toward higher energies, thus less included in the BW; (ii) the transmission peaks are decreased. Consequently, the current in presence if AFB1 is reduced. Fig. 4(b) reports the $T(E, V_{DS})$ in presence and absence of AFB1 for $V_{DS} = 1$ V. Notice that since $T(E, V_{DS})$ depends on V_{DS}, it differs from the one in Fig. 4(a). The effect of AFB1 is again to shift up the transmission peaks and lower the main one within the BW. Consequently, the portion of $T(E, V_{DS})$ included within the BW and thus the current are lowered.

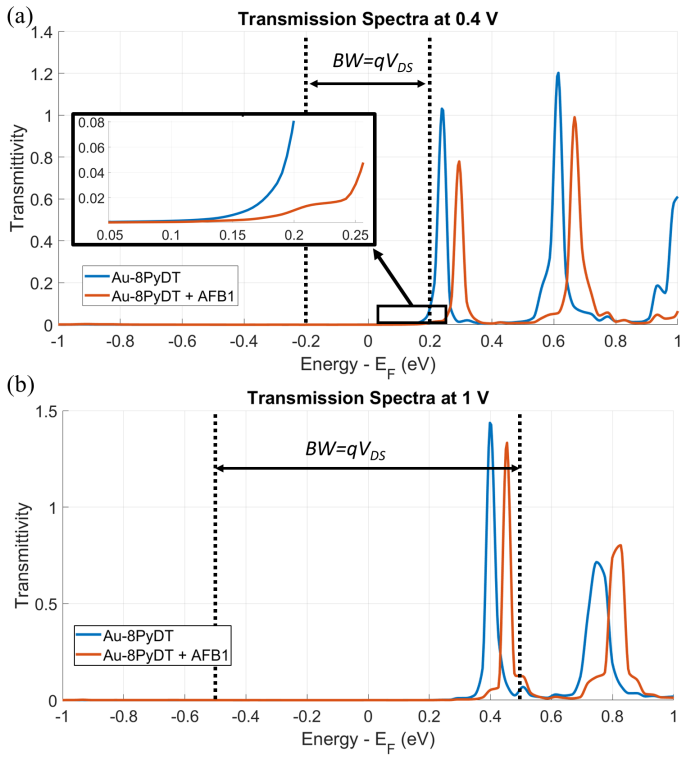

Fig. 4. $T(E)$ of the Au-8PyDT with and w/o AFB1 at fixed V_{DS}=0.4 V (a) and at fixed V_{DS}=1 V (b). The inset in (a) shows an enlargement around 0.2 eV.

IV. Conclusion

We investigated the Au-8PyDT molecular quantum dot as an amperometric Single-Molecule Sensor (SMS) for the AFB1 detection. Our results show that the presence of AFB1 can significantly modulate the current flowing in the Au-8PyDT molecular dot with an interesting voltage-dependent sensor response. We suppose this feature can pave the way toward re-configurable sensors detecting various analytes at different V_{DS} values, as we resolve to investigate in future works. At the moment, we identify two possible operating voltages for AFB1 amperometric detection, namely 0.4 V and 1 V, providing a percentage current modulation of 83.87% and 29.6% and an absolute deviation of 0.26 µA and 0.626 µA. Current variations of this order are proved to be measurable through integrated CMOS front-end electronics. The proposed sensing technique thus opens the way toward label-free, *in-situ*, real-time and automatic monitoring of AFB1 concentration in food stocks and on field. Thanks to the pyrrole non-toxicity and simple synthesis process, the explored Au-8PyDT is thus promising for future investigations as SMS of AFB1, achieving the potential single-molecule sensitivity.

References

[1] W. H. Organization and S. Joint FAO/WHO Expert Committee on Food Additives (83rd, 2017: Geneva, *Evaluation of certain contaminants in food: eighty-third report of the Joint FAO/WHO Expert Committee on Food Additives*. World Health Organization, 2017.

[2] IARC Working Group on the Evaluation of Carcinogenic Risks to Humans, "Some traditional herbal medicines, some mycotoxins, naphthalene and styrene," *IARC Monogr Eval Carcinog Risks Hum*, vol. 82, pp. 1–556, 2002.

[3] C. Yan, Q. Wang, Q. Yang, and W. Wu, "Recent advances in aflatoxins detection based on nanomaterials," *Nanomaterials*, vol. 10, no. 9, 2020.

[4] Z. Xue, Y. Zhang, W. Yu, J. Zhang, J. Wang, F. Wan, Y. Kim, Y. Liu, and X. Kou, "Recent advances in aflatoxin b1 detection based on nanotechnology and nanomaterials-a review," *Analytica Chimica Acta*, vol. 1069, pp. 1–27, 2019.

[5] J. J. Gooding and K. Gaus, "Single-molecule sensors: Challenges and opportunities for quantitative analysis," *Angewandte Chemie International Edition*, vol. 55, no. 38, pp. 11 354–11 366, 2016.

[6] Y. Li, C. Yang, and X. Guo, "Single-molecule electrical detection: A promising route toward the fundamental limits of chemistry and life science," *Accounts of Chemical Research*, vol. 53, no. 1, pp. 159–169, 2020, pMID: 31545589.

[7] N. Xin, X. Li, C. Jia, Y. Gong, M. Li, S. Wang, G. Zhang, J. Yang, and X. Guo, "Tuning charge transport in aromatic-ring single-molecule junctions via ionic-liquid gating," *Angewandte Chemie International Edition*, vol. 57, no. 43, pp. 14 026–14 031.

[8] F. Mo, C. E. Spano, Y. Ardesi, G. Piccinini, and M. Graziano, "Beyond-CMOS artificial neuron: A simulation- based exploration of the molecular-FET," *IEEE Transactions on Nanotechnology*, vol. 20, pp. 903–911, 2021.

[9] V. Cauda, P. Motto, D. Perrone, G. Piccinini, and D. Demarchi, "ph-triggered conduction of amine-functionalized single ZnO wire integrated on a customized nanogap electronic platform," *Nanoscale Res. Lett.*, vol. 9, no. 1, p. 53, Jan. 2014.

[10] G. M. Whitesides and M. Boncheva, "Beyond molecules: Self-assembly of mesoscopic and macroscopic components," vol. 99, no. 8, pp. 4769–4774, 2002.

[11] A. Fahlgren, C. Bratengeier, A. Gelmi, C. M. Semeins, J. Klein-Nulend, E. W. H. Jager, and A. D. Bakker, "Biocompatibility of polypyrrole with human primary osteoblasts and the effect of dopants," *PloS one*, vol. 10, no. 7, pp. e0 134 023–e0 134 023, Jul 2015, 26225862[pmid].

[12] X. Wang, X. Gu, C. Yuan, S. Chen, P. Zhang, T. Zhang, J. Yao, F. Chen, and G. Chen, "Evaluation of biocompatibility of polypyrrole in vitro and in vivo," *J Biomed Mater Res A*, vol. 68, no. 3, pp. 411–422, Mar. 2004.

[13] T. V. Vernitskaya and O. N. Efimov, "Polypyrrole: a conducting polymer its synthesis, properties and applications," *Russian Chemical Reviews*, vol. 66, no. 5, pp. 443–457, may 1997.

[14] A. Dimonte, S. Frache, V. Erokhin, G. Piccinini, D. Demarchi, F. Milano, G. D. Micheli, and S. Carrara, "Nanosized optoelectronic devices based on photoactivated proteins," *Biomacromolecules*, vol. 13, no. 11, pp. 3503–3509, 2012.

[15] F. Neese, "The orca program system," *WIREs Computational Molecular Science*, vol. 2, no. 1, pp. 73–78, 2012.

[16] S. Smidstrup, T. Markussen, P. Vancraeyveld, J. Wellendorff, J. Schneider, T. Gunst, B. Verstichel, D. Stradi, U. Martinez, A. Blom, M. Brandbyge, and K. Stokbro, "QuantumATK: an integrated platform of electronic and atomic-scale modelling tools," *Journal of Physics: Condensed Matter*, vol. 32, no. 1, p. 015901, oct 2019.

[17] S. Datta, *Quantum Transport: Atom to Transistor*, 2005, doi: 10.1017/CBO9781139164313.

[18] A. Zangwill, *Physics at Surfaces*. Cambridge University Press, 1988.

[19] T. Steiner, "The hydrogen bond in the solid state," *Angewandte Chemie International Edition*, vol. 41, no. 1, pp. 48–76, 2002.

[20] F. Ciriaco, V. De Leo, L. Catucci, M. Pascale, A. F. Logrieco, M. C. DeRosa, and A. De Girolamo, "An in-silico pipeline for rapid screening of dna aptamers against mycotoxins: The case-study of fumonisin b1, aflatoxin b1 and ochratoxin a," *Polymers*, vol. 12, no. 12, 2020.

[21] L. Ma, J. Wang, and Y. Zhang, "Probing the characterization of the interaction of aflatoxins b1 and g1 with calf thymus dna in vitro," *Toxins*, vol. 9, no. 7, p. 209, Jul 2017, 28671585[pmid].

[22] C.-L. Hsu and D. A. Hall, "A current-measurement front-end with 160db dynamic range and 7ppm inl," in *2018 IEEE International Solid - State Circuits Conference - (ISSCC)*, 2018, pp. 326–328.